Emission of Volatile Organic Compounds to the Atmosphere from Photochemistry in Thermokarst Ponds in Subarctic Canada

Daniel Fillion, Sébastien Perrier, M. Riva, C. George, Florent Domine, Raoul-Marie Couture

Emission of volatile organic compounds to the atmosphere from photochemistry in thermokarst ponds in subarctic Canada

Daniel Fillion[1,2], Sébastien Perrier[3], Matthieu Riva[3], Christian George[3], Florent Domine[1,2] and Raoul-Marie Couture[1,2,*]

[1] Centre d'études nordiques and Department of Chemistry, Université Laval, 2325 Rue de l'Université, Québec, QC, Canada, G1V 0A6

[2]Takuvik Joint International Laboratory, Université Laval and CNRS-INSU (France), 2325 Rue de l'Université, Québec, QC, Canada, G1V 0A6

[3]Univ Lyon, Université Claude Bernard Lyon 1, CNRS, Ircelyon, 69626, Villeurbanne, France

Correspondance : raoul.couture@chm.ulaval.ca

Keywords : cold region, permafrost, carbon cycle, dissolved organic matter, VOCs, Vocus PTR-TOF.

Abstract

Climate warming is accelerating the thawing of permafrost, which contains almost twice as much carbon as the atmosphere, to a point where a large quantity of dissolved organic matter (DOM) is being mobilized toward surface waters including thermokarst ponds. DOM can be partially photo-degraded into volatile organic compounds (VOCs) which are little studied in Arctic environments. The main objective of this work is to identify and quantify the VOCs emitted to the gas phase by photochemistry from thermokarst water sampled in four ponds from two study sites in northern Quebec. VOC emissions were characterized by proton-transfer-reaction mass spectrometry. Results show rapid photoproduction of between 35 and 59 VOCs when dissolved organic matter (DOM) water samples are exposed to radiation. Our results also show that the quality of DOM is a more important factor to control VOC photoproduction than the quantity of DOM. Depending

on the assumptions used in upscaling our laboratory results to the field sites, calculations yield net carbon fluxes, between 1.93 and 174 μmol C m^{-2} d^{-1} . While these values are small compared to literature values of CO_2 and CH_4 fluxes from thermokarst ponds, this process represents an important flux of reactive molecules that could affect Arctic atmospheric chemistry.

1. Introduction

The Arctic is warming at a rate nearly four times faster than other regions of the globe [1]. This acceleration affects northern environments in drastic ways, intensifying geomorphological changes such as permafrost thaw and subsequent formation of thermokarst ponds [2, 3]. Since permafrost contains almost twice as much carbon as the atmosphere [4], its erosion leads to the transfer of organic material to surface waters including thermokarst ponds. These ponds become important natural bio- and photochemical reactors where these organic molecules are mineralized, resulting in CO_2 and CH_4 emissions to the atmosphere [5].

Photochemical degradation, which includes photolysis and photosensitization, is a major pathway of DOM processing in northern inland waters, and photolysis rates are relevant to the Arctic carbon cycle [6-9]. Terrestrial DOM is rich in chromophoric DOM (CDOM), the light-absorbing fraction of DOM, which is composed of high molecular weight, aromatic and colored compounds. Complete and partial photo-oxidation of CDOM produce CO_2 and partially oxidized carbon compounds, respectively [10-12]. Product molecules are generally more aliphatic and, being broken down, have a lower molecular mass than their precursor. Their fate is generally insufficiently understood in aquatic systems [13].

Here, we test the hypothesis that some partially oxidized photoproducts are sufficiently volatile to be emitted as volatile organic compounds (VOCs) to the atmosphere. This would add another pathway for C evasion from thermokarst ponds in addition to those listed above. While small molecules, such as acetone, formaldehyde, pyruvic acid and acetaldehyde are photoproduced in the liquid phase [13-15], their transfer to the gas phase has not been documented in the Arctic. Given that Brüggemann et al. [16] reported that the photolysis of humic substances at the sea–air interface could lead to the significant production of various VOCs, we suggest that similar processes in thermokarst ponds deserve investigation.

VOCs are produced from a wide range of natural and anthropogenic sources and are ubiquitous in the environment [17]. Yet, their sources in the Arctic have not been studied extensively. To our knowledge, only a few papers focus on VOC emissions from thawing permafrost soil [18-22] and marine systems [23, 24]. In the atmosphere, VOCs further undergo a series of oxidative chemical processes leading to the formation of secondary organic aerosols (SOA) [25]. Since SOA can act as cloud condensation nuclei (CCN) [26], these transformations increase water droplet formation within a cloud, which increases cloud albedo. This process is known as the Twomey effect or the indirect aerosol effect [27]. VOCs can also contribute to tropospheric ozone (O_3) and production of radicals (e.g., OH, HO_2) [28, 29].

Thus, VOCs could be a reservoir of C that represents a delayed source of greenhouse gases (GHGs) $CO_{2(g)}$ and $O_{3(g)}$ from thermokarst ponds to the atmosphere. This source is not currently accounted for as studies have focused on direct flux measurements above the pond [30-33]. Laboratory experiments are necessary to isolate photoproduction since field

measurements alone cannot discern the precise origins (cyanobacteria, algae, sunlight) [34]. This study aims to fill this knowledge gap by examining and quantifying the photolytic formation of VOCs in thermokarst ponds. To this end, we conducted photo-degradation experiments on water samples collected in thermokarst ponds from two subarctic regions. We have estimated VOC emissions using a proton-transfer-reaction time-of-flight mass spectrometry (Vocus® PTR-ToF-MS). We compare the fluxes of VOCs to literature values of CO_2 and CH_4 fluxes from subarctic thermokarst ponds. We have also tested the hypothesis that samples with higher CDOM content might lead to a wider variety and greater fluxes of photoproduced VOCs, due to the observation that DOM photo lability is related to its chemical composition [12, 35, 36].

We build on our previous preliminary exploration[37] that demonstrated the feasibility of detecting VOCs from photolysis of natural pond water. Relying on a similar methodology, we have extended field sampling to four ponds, collecting samples at various depths as well as riparian water. Furthermore, we filtered (0.2 μm) some samples on site to assess the impact of particulate matter on photolysis products. Laboratory work was also expanded to test experimental variables such as dissolved oxygen and exposure time. This contribution thus provides a clearer basis upon which to evaluate field-relevant VOC generation in subarctic regions.

2. Methodology

2.1. Study sites and selected ponds

The water column was sampled from four ponds located in two locations selected based on their contrasting organic matter composition and concentrations in the aquatic

environment: Tasiapik Valley (TAS; 56.56° N, 76.48° W) and Sasapimakwananistikw River Valley (SAS; 55.13° N, 77.41° W) (Figure 1). Both locations are on the eastern coast of the Hudson Bay in Nunavik (northern Quebec, Canada). Thermokarst ponds at TAS are formed from the collapse of lithalsas, which are small permafrost mounds with an organic-poor cover [38]. In contrast, thermokarst ponds at SAS are formed following the collapse of peat-covered permafrost mounds called palsas [39].

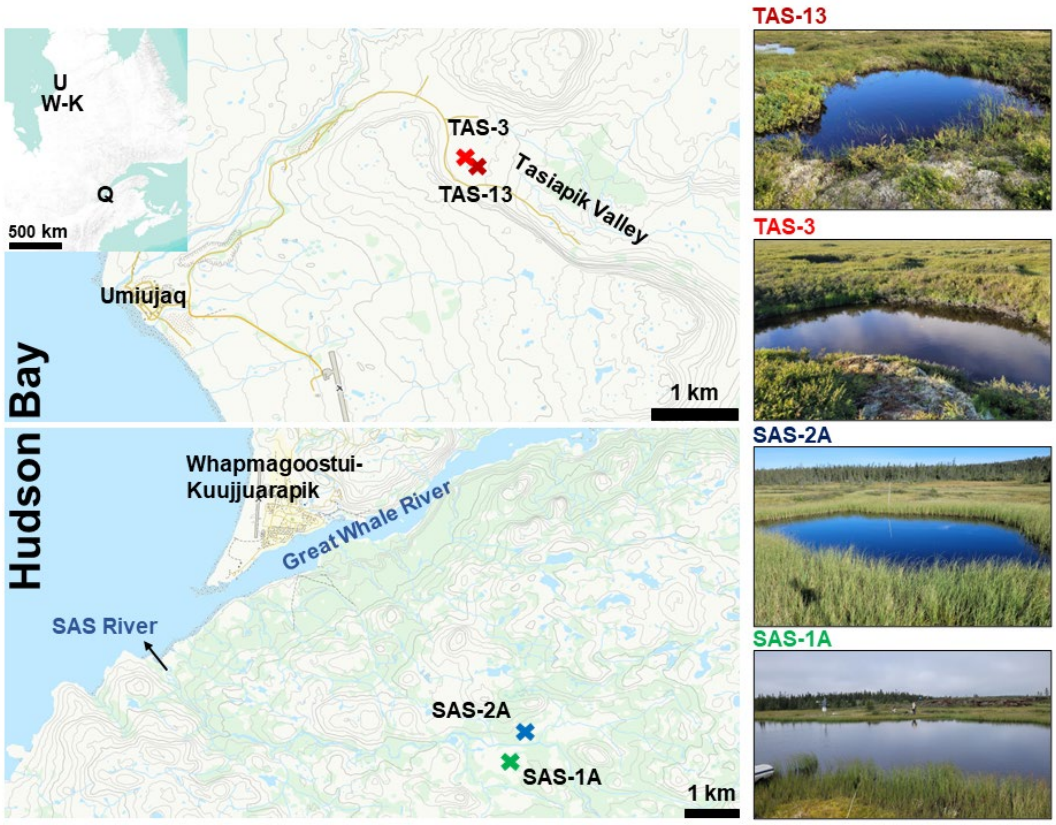

Figure 1. Study sites locations on the Hudson Bay coast in northern Quebec along with photos of selected ponds. U = Umiujaq, W-K = Whapmagoostui-Kuujjuarapik, Q = Quebec City. Maps adapted with permission from HRDEM - CanElevation Series[40].

106 The selected ponds at Tasiapik Valley are in the discontinuous permafrost region in the
107 upper part of the valley, 5 km east of the village of Umiujaq. This area has sandy soils with
108 low concentrations of soil organic carbon [38]. As a result, thermokarst ponds at this site are
109 poor in CDOM. To our knowledge, there are no published data on the physicochemistry of
110 the TAS ponds. The two ponds selected are TAS-3 (56.3336° N, 76.2887° W) and TAS-
111 13 (56.3346° N, 76.2862° W) (Figure 1). TAS-3 is located at the bottom of a collapsing
112 lithalsa and has yellow water color while TAS-13 is further away from the lithalsas and has
113 clearer water. Both ponds were shallow with a maximum depth of 1.9 m for TAS-3 and 0.8
114 m for TAS-13. Their surface area was not measured but it was less than 100 m^2 for both
115 ponds. Riparian waters were also sampled at the site, about 30 m upstream from TAS-3
116 (56.3351° N, 76.2875° W). Also, thermokarst ponds in the Tasiapik Valley have not been
117 characterized extensively in the literature, thus the thermokarstic origin of TAS-13 cannot
118 be confirmed (I. Laurion, pers. comm), although its presence near a collapsing lithalsa and
119 its high DOM concentrations leads us to believe that it is.

120 The SAS valley is located in a peatland, at the northern limit of the sporadic permafrost
121 zone, 8 km southwest of the village of Whapmagoostui-Kuujjuarapik. Permafrost occupies
122 only 2% of the surface and is contained in the palsas. Thermal erosion, which started 150
123 years ago, is responsible for palsa collapse [39]. Consequently, the site contains many dark-
124 colored thermokarst ponds rich in terrigenous organic matter [41], leading to strong light
125 attenuation in the water column [9]. The selected ponds are SAS-1A (55.1301° N, 77.4203°
126 W) and SAS-2A (55.1304° N, 77.4105° W), located on opposite sides of the SAS river
127 (Figure 1). Pond SAS-1A has a surface area of 1661 m^2 and a depth of 1.3 m. Pond SAS-
128 2A is smaller but deeper, with an area of 104 m^2 and a maximum depth of 2.5 m. Again,

129 riparian waters were also sampled, approximately 20 m away from SAS-2A (55,1360° N,
130 77,4181° W). DOC characterization and CO_2/CH_4 emissions have been studied at both
131 ponds [33, 42].

132 **2.2. Sample Collection and in situ Measurements**

133 TAS was visited on August 8–9th 2022 and SAS on August 12–13th 2022. Prior to water
134 sampling, vertical profiles of physicochemical properties (temperature, pH, dissolved O_2
135 and conductivity) were measured using a RBR Concerto® equipped with the relevant
136 sensors. At the TAS valley, however, only the surface temperature was measured. Water
137 samples were retrieved with a 2-L Van Dorn bottle and delivered to amber bottles (60 and
138 250 mL) that were previously cleaned for 4 hours in HCl (10%), 12–16 hours in NaOH (5
139 mM) and baked for 3 hours at 450 °C to remove residual organics. The bottles were
140 thoroughly washed with MilliQ water (18 MΩ) between each of those steps.

141 Before sampling, the bottles were rinsed three times with pond water to saturate sorption
142 sites at the surface of the glassware. Surface samples for total organic carbon (TOC) and
143 dissolved organic carbon (DOC) were taken at all sites, with additional bottom samples at
144 SAS-1A as well as middle and bottom samples at SAS-2A. At TAS, a riparian water sample
145 was collected by digging a hole ~80 cm deep near the ponds and sampling the water that
146 filled the hole. At SAS, it was possible to simply open the floating wetland vegetation to
147 retrieve a riparian sample.

148 Samples for TOC analysis were delivered directly to a 250-mL bottle without filtering,
149 while samples for DOC analysis were filtered on a 0.2-µm polyethersulfone (PES) syringe
150 filter into a 60-mL bottle. Field blanks were also taken by applying the same protocol using

MilliQ water (18 Ω). All bottles were filled to the top to minimize air–water interaction and kept at 4 °C until analysis. TOC and DOC analysis occurred within two weeks of sample collection while photolysis experiments occurred four months after sample collection. They were kept sealed until the analysis. Note that the TOC sample from SAS-2A (middle) is missing due to it being damaged during transportation back to the laboratory.

2.3. DOM Characterization

TOC and DOC concentrations were measured using a Total Organic Carbon analyzer (Vario TOC Cube, Elementar) calibrated with potassium hydrogen phthalate (KHP) standards. Particulate organic carbon (POC) was calculated as the difference between TOC and DOC.

Prior to DOC analysis, a suite of chromophoric properties, collectively referred to as DOC quality, were assessed. First, CDOM was characterized using absorbance scans acquired between 200 and 700 nm with a 1 nm increment on a UV–Vis spectrophotometer (Aqualog, Horiba, USA). A 1-cm path length fused silica UV-transparent cuvette was used. The samples were allowed to reach room temperature prior to analysis. A blank of MilliQ water (18 MΩ) was done every 10 samples as a reference and subtracted from the sample. The absorbance values were then converted to absorption coefficients a_λ (m^{-1}) using:

$$a_\lambda = \frac{\ln(10) \times A_\lambda}{L} \quad (1)$$

where A_λ is the absorbance value at a specific wavelength and L is the optical path length in meters, here 0.01 m.

The indicator a_{320} was used as a proxy to measure the concentration of CDOM [43]. $SUVA_{254}$, the specific UV absorbance at 254 nm normalized to DOC concentrations, was calculated as an indicator of the aromatic content [44]. Finally, the ratio of the slopes between 275–295 nm and 350–400 nm, a metric called the slope ratio (Sr), is inversely proportional to the molecular size [45] and was obtained using the R package CDOM by Massicotte and Markager [46].

2.4. Photolysis Experiments

The experimental set-up for photolysis experiments was adapted from a previously published design [16, 47]. Briefly, a 5-cm high custom Pyrex photoreactor with the axis placed vertically was equipped with a fused silica window (Figure 2). The reactor had a truncated conical shape with a diameter of 4 cm at the top and 5 cm at the bottom. It was positioned under a Xenon arc lamp (150 W, QuantumDesign, France) mounted before a water filter to simulate solar irradiation ($\lambda > 280$ nm). This lamp was chosen as it is suitable for aquatic photodegradation studies[48]. Its irradiance spectrum is shown in Figure S3. A mirror reflected the incident beam to irradiate the reactor from the top. A constant flow of 300 mL min^{-1} of ultrapure N_2 flowed through the reactor as a carrier gas to bring VOCs to the mass spectrometer. To ensure anoxia in the photoreactor, the samples were kept under an N_2 atmosphere for at least 10 minutes before starting an experiment, which is sufficient given the 10 seconds flush rate. A N_2 atmosphere was chosen first to investigate photolysis under anoxic conditions, which are ubiquitous in poorly mixed, and thus strongly stratified, thermokarst ponds [49, 50]. Experiments under oxic conditions were performed with a 20:80 mix of O_2 and N_2. Perfluoralkoxy (PFA) tubing used throughout was rinsed with ethanol and MilliQ water then baked at 120 °C for 3 hours. The sample temperature was maintained

at 10 °C using a cryostat to ensure temperature representative of summer water [51]. Although we did not test it directly in this study, previous work relying on a similar photochemical apparatus showed no significant changes in temperatures throughout the experiment (Wang et al., 2023). A typical experiment contained 15 mL of water sample and began with 30 minutes of stabilization period, after which the lamp was turned on for 90 minutes, and it ended with another 30 minutes of stabilization without light. Both TOC and DOC water samples were analyzed using this experimental set-up.

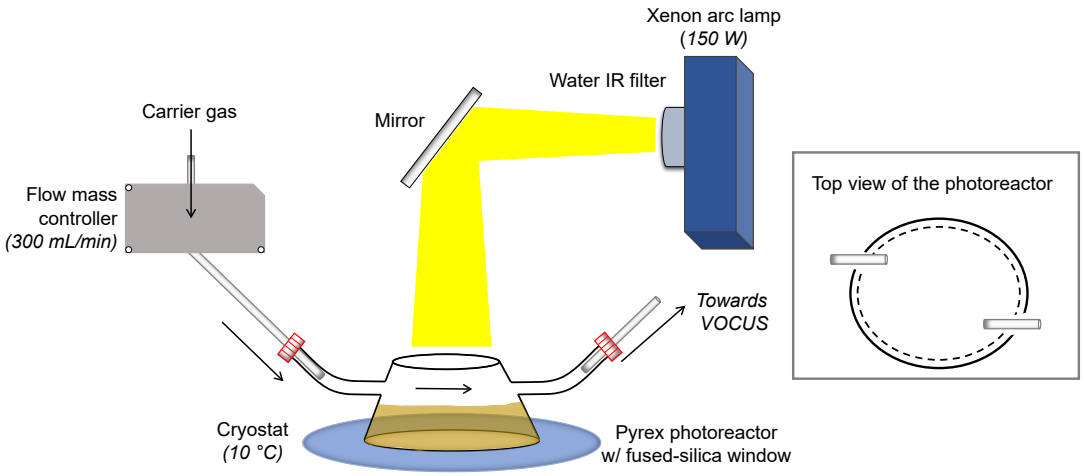

Figure 2 Experimental set-up used for photochemistry experiments. Black arrows indicate the direction of the carrier gas. The solid and dotted lines on the top view of the photoreactor show the bottom and top of the reactor, respectively.

2.5. Mass Spectrometry

A Vocus proton-transfer-reaction time-of-flight mass spectrometry (Vocus; Tofwerk AG) was used to analyze and quantify the VOCs emitted from the photolysis of DOM in thermokarst samples. Compared with traditional PTR mass spectrometers, the Vocus has a better mass resolution and detection efficiency due to implemented attributes such as an improved inlet and source design that minimize contact between analytes and the source walls [52]. Thus, it can detect chemical species with concentrations in the pptv range with a

mass resolving power of 10 000 m/Δm [53]. The ionization reagent was hydronium ions (H_3O^+) which allows the detection of a wide range of functional groups [53].

Five sccm of a custom calibration standard were diluted into a 250 sccm flow of clean air to calibrate the instrument twice a day. The standard was made of the following five VOCs in N_2: acetone (240 ppb), benzene (250 ppb), xylene (175 ppb), chlorobenzene (155 ppb) and α-pinene (165 ppb). Blank measurements were routinely conducted on the reactor filled with 15 mL of MilliQ water. Data treatment, mass calibration, peak fitting and time series plotting was performed using Tofware v.3.2.2 within the IGOR 7.0 environment (WaveMetrics). A product ion was assigned as a VOC if its blank-subtracted signal increased at least 3-fold after the lamp was turned on. To simplify chemical formula assignment, only compounds having C (0–20 atoms), H (0–40), O (0–20), N (0–5), S (0–2) and P (0–2) were considered. Then, molecular formulae were determined using Tofware's high-resolution assignment tool. Methods to extract molecular information from the PTR-MS masses can be found elsewhere[54, 55]. It is worth noting that such mass spectrometry technique does not allow us to confirm the structure of the molecules obtained since different isomers can exist for a given stoichiometry. The chemical composition is tentatively assigned to compounds but might arise from other compounds fragmenting in the PTR source [56]. Hence, the term "candidate" is used throughout.

To characterize VOCs, five metrics were calculated, namely the H:C and O:C ratios, ring double-bond equivalent (RDBE), modified aromaticity index (AI_{mod}) and the carbon oxidation state (OS_c). A detailed description of these indicators can be found in the SI.

2.6. Flux Calculations

PTR-MS is a method that allows, in principle, the estimation of VOC concentrations without external calibration, notably when the protonation reaction rate constants (k_p) are known [57, 58]. This is due to k_p being linearly related to the sensitivity (in counts per ppb of analyte) of the instrument [58]. A method to calculate the concentrations of uncalibrated compounds based on this relationship is described in Yuan, Koss, Warneke, Coggon, Sekimoto and de Gouw [59]. Briefly, a calibration curve between the sensitivities and k_p of the five calibrants used was constructed (Figure S1 in supplementary information). This linear equation (sensitivity (cps/ppb) = m x k_p, where m is the slope) was used to estimate the sensitivity of uncalibrated compounds, which can then be used to estimate concentrations. The calculated sensitivities have an error range between 50–100 % due to potential side reactions (e.g.,ligand transfer with water cluster) and the ion transmission efficiency in the ionization source [52]. Because we cannot be certain of the identity of the compounds, an average value of $2x10^{-9}$ molecules cm^3 s^{-1} was chosen [57]. The concentration of a VOC was calculated by taking the maximum signal obtained during the experiment and subtracting the average background signal 5 minutes before irradiation.

Carbon fluxes (nmol C m^{-2} s^{-1}) associated with VOC formation from the reactor were calculated using two different approaches. Approach 1 is based on equations 2 and 3 while Approach 2 is based on Equation 4. First, we converted carbon fluxes into µmol C m^{-2} d^{-1} to facilitate comparisons with other studies:

$$\text{Flux} = \sum \frac{f \times C_i \times N_i \times 10^{-3}}{A \times V_t} \quad (2)$$

where f = flow rate of the vector gas (1.67 mL s^{-1}), C_i = concentration of one VOC (ppb), N_i = number of C atoms in the VOC chemical formula, V_t = molar volume of gas (24.4 L mol^{-1}), A = area of surface exposed to irradiation (0.00196 m^2).

Then, to estimate fluxes in the field, we corrected the fluxes ($Flux_{corr.}$) to account for the natural irradiance in the field as follows:

$$Flux_{corr.} = Flux \times \frac{E_{field}}{E_{laboratory}} \quad (3)$$

where E_{field} is the average of natural irradiance values obtained in the field in Tasiapik Valley, near the sampling site, during the warm season of 2021 (May 1st to August 30th). They were measured hourly at a meteorological station (56.5592° N, 76.4821° W) equipped with a radiometer (CNR4; Kipp & Zonen) sensitive to the wavelength range 300–2800 nm. The spectral distribution was obtained from simulated spectral data (Figure S2) and the range between 300 and 400 nm was chosen since it is the most relevant for photochemistry [60]. The dataset was published by Lackner et al. [61]. Since SAS and TAS are only 167 km apart and can be thought to receive similar seasonal photon fluxes, TAS data was used for both sites. Moreover, $E_{laboratory}$ is the irradiance output from the lamp normalized to the surface area of the reactor and gives a value of 5.73 W/m^2 for the range 300-400 nm (Figure S3). Finally, the exact transfer function to link our experimental light irradiation to the natural light is unknown, we assumed that this relationship was linear.

Since flux calculations based on Approach 1 do not account for CDOM absorption or water column attenuation, we also upscaled VOCs emissions based on a photolysis rate provided in Cory and Kling (2018), bearing mind the uncertainty in the value of the apparent quantum yield:

$$\text{Flux} = \int_{300\ \text{nm}}^{400\ \text{nm}} \Phi_\lambda E_\lambda ((1 - e^{-K_d}) \frac{a_{CDOM,\lambda}}{a_{total,\lambda}} \quad (4)$$

Where Φ_λ is the apparent quantum yield of the gaseous products, E_λ is the sunlight absorption by CDOM, K_d is the attenuation coefficient (data at SAS and TAS from I. Laurion, pers. comm.), $a_{CDOM,\lambda}$ is the absorption coefficient of the CDOM at a specific wavelength (350 nm) and $a_{total,\lambda}$ is the total light absorbed.

3. Results

3.1. DOM properties of the selected ponds

DOC concentrations vary among sites and with depth, with bottom samples having higher DOC concentrations than surface samples (Table 1). The highest values were at the bottom of SAS-2A. SAS ponds also had a higher TOC content with a lower proportion of POC (0–8% POC) than the TAS ponds (13–38% POC).

CDOM characterization reveals that SAS-2A (bottom) showed high values for the indicators a_{320} and $SUVA_{254}$, along with lowest Sr values, establishing that it is likely the most photo-labile sample. Overall, the values for a_{320} range between 8.63 and 303 m^{-1}, with the highest values measured at SAS. $SUVA_{254}$ values at SAS (5.14-6.01L mg C^{-1} m^{-1}) are in a similar range than at TAS (2.58-7.60L mg C^{-1} m^{-1}). TAS samples cover a wider range of Sr values than the samples at SAS, ranging from 0.54, in TAS-13, to 0.97 in TAS-3. Sr values were grouped between 0.62 and 0.80 at SAS. Finally, riparian samples show relatively low $SUVA_{254}$ (5.93 L mg C^{-1} m^{-1}) and a_{320} values (8.63–43.6 m^{-1}).

Site/pond	ID	Depth	[TOC]	[DOC]	[POC]	a_{320}	$SUVA_{254}$	Sr
-	-	cm	ppm	ppm	ppm	m^{-1}	L mg C^{-1} m^{-1}	-
SAS-2A	S	25	5.61	5.28	0.33	78.0	5.56	0.76
	M	125	-	13.9	-	162	5.30	0.66
	B	225	28.1	25.8	2.3	303	6.01	0.62
SAS-2A	Rip.	-	19.6	-	-	43.3	-	0.72
SAS-1A	S	25	8.27	7.78	0.49	91.6	5.14	0.80
	B	125	14.9	15.0	<DL	170	5.25	0.69
TAS-3	S	25	14.6	9.14	5.5	49.7	3.45~~7.95~~	0.84
TAS-13	S	25	6.01	5.19	0.82	63.3	7.60	0.54
TAS	Rip.	-	-	2.89	-	8.63	2.58	0.90

Table 1 Concentrations of TOC, DOC and POC and chromophoric indices calculated from UV–Vis spectra obtained for each DOC sample (0.2 µm-filtered sample). (TOC = total organic carbon; DOC = dissolved organic carbon; POC = particulate organic carbon; a_{320} = absorption coefficient at 320 nm; $SUVA_{254}$ = specific ultraviolet absorption at 254 nm; Sr = slope ratio; S = surface; M = middle; B = bottom; Rip. = riparian, DL = detection limit).

3.2. Photolysis Experiments

In all experiments, VOC production started immediately when the lamp was switched on (Figure 3). Two kinds of behavior were observed; in the first, the signal reached a maximum after a few minutes and then decreased constantly or remained relatively stable (i.e., SAS-2A). In the second, the signal continuously increased (i.e., TAS-3 or SAS-2A riparian). The photoproduction stopped when the lamp was switched off, with the signal decaying and returning to background levels after about 30 minutes. The irradiation of

MilliQ water also showed some VOC production (Figure S4), which was expected since the experimental set-up comprises different porous plastic materials and tubing. The repeatability of the method was assessed by a triplicate done on the SAS-2A bottom sample (Figure S5).

Two additional tests were performed to further investigate the extent of VOC photoproduction. First, a longer exposure to irradiation demonstrated that about 2–3 hours were required to deplete all the reactants in the TAS-3 surface sample (Figure 3d). Second, we evaluated the effects of dissolved oxygen on VOC photoproduction under an oxic atmosphere (20:80 mix of O_2 and N_2) for SAS-2A (surface, DOC). The time series obtained (Figure 3e) shows a pattern similar to that under a N_2 atmosphere, albeit with a weaker signal.

After blank subtraction, the total number of VOCs detected by the Vocus from the samples among all ponds ranged between 35 and 59 species (Figure 4) with 26 molecular masses being common to all experiments. The TOC samples (non-filtered water) produced fewer VOCs than the DOC samples (0.2 μm-filtered), except for TAS-3 where 6 additional VOCs were produced by the TOC sample. Only one S compound (m/Q of 49.011, tentatively assigned to $CH_4S\text{-}H^+$) was detected while no P-containing molecules were detected (Table S1 and Table S2).

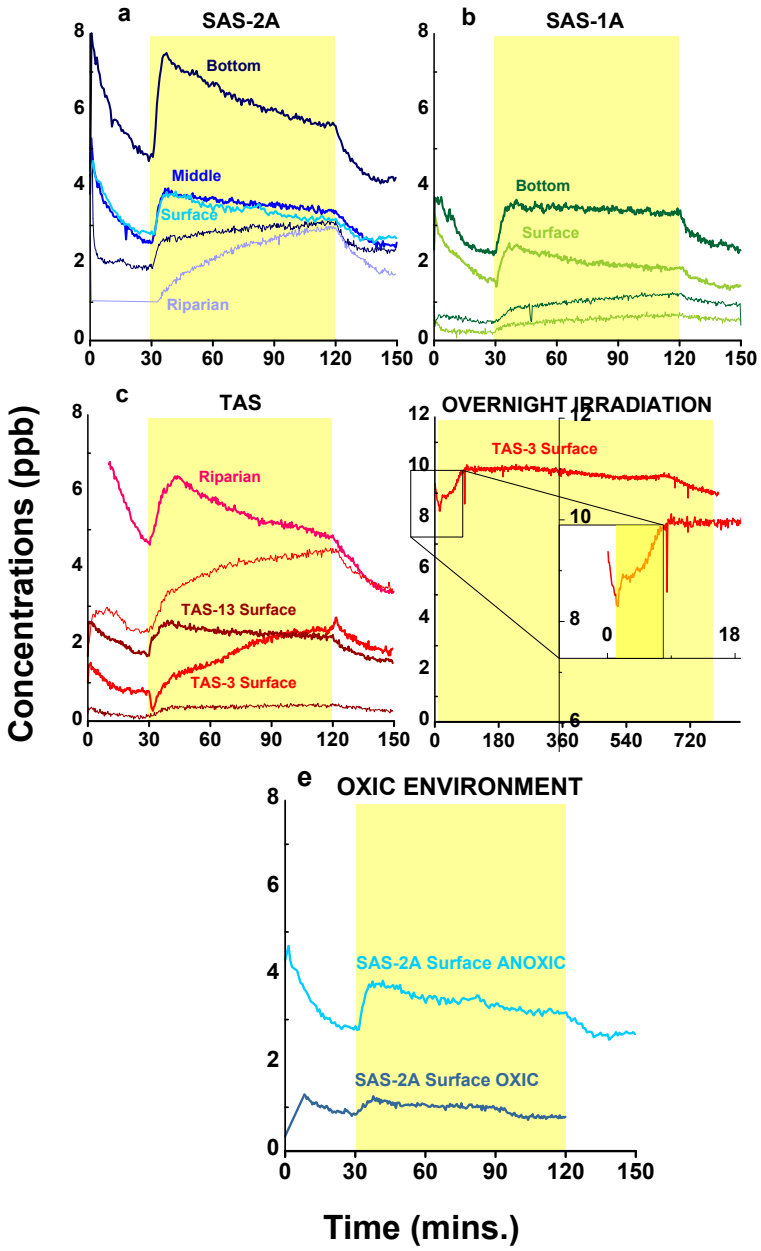

Figure 3 Blank-subtracted time series of all VOCs produced from each sample at (a) SAS-2A (b) SAS-1A, (c) TAS (d) Time-series (not blank subtracted) when TAS-3 (surface) is irradiated for 13 hours. The yellow rectangle corresponds to the irradiation window (90 minutes for anoxic experiments and 60 minutes for the oxic experiment). The thick line corresponds to the DOC samples and the thin line refers to the TOC samples. (e) Comparison between oxic and anoxic environment for the sample SAS-2A (surface).

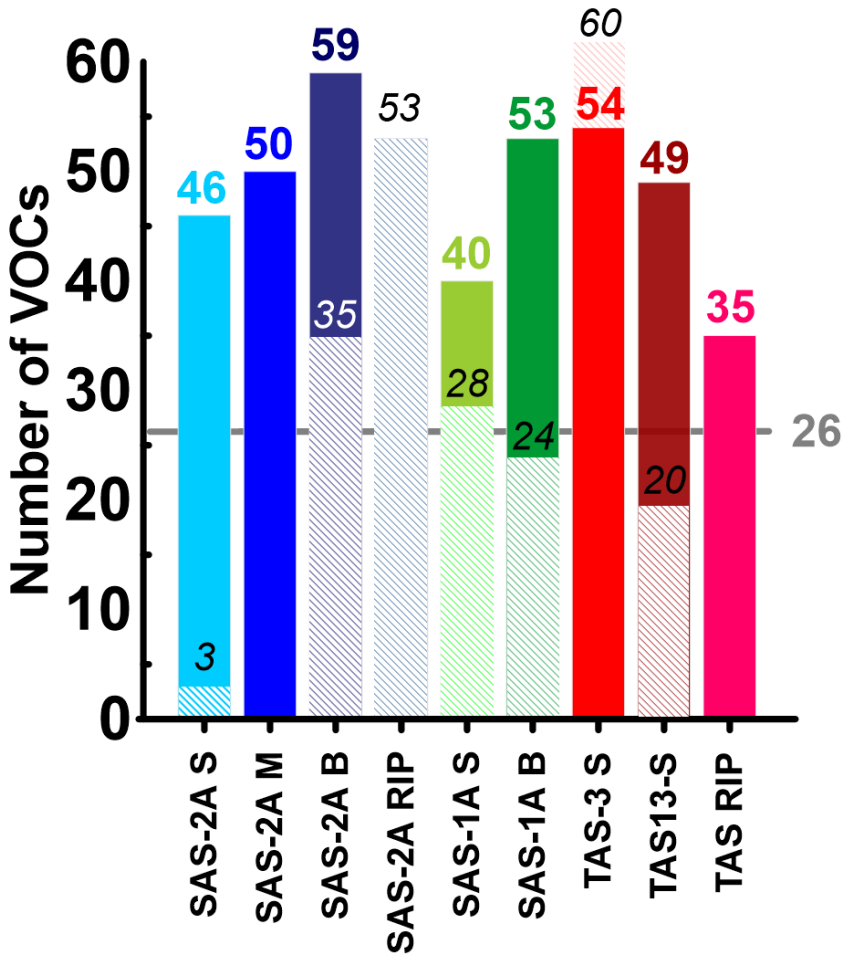

339

340 **Figure 4** Total number of VOCs detected for each sample at both study sites. The
341 horizontal grey line represents the 26 VOCs common to all samples. The dashed boxes
342 with italic numbers show the VOCs detected from TOC samples.

343 The metrics used to characterize VOCs are listed in Table 2. In general, VOCs from SAS
344 contained more oxygen atoms than those from TAS, as illustrated by their higher O:C ratio
345 and OS_c values. RDBE and AI_{mod} values were higher at TAS-3. H:C values ranged between
346 1.79 and 1.84 among all ponds.

Site/pond	ID	O:C		H:C		RDBE		AI_{mod}		OS_c	
		DOC	TOC	DOC	TOC	DOC	TOC	DOC	TOC	DOC	TOC
	S	0.27	-	1.81	-	1.93	-	0.25	-	-1.28	-
SAS-2A	M	0.28	-	1.79	-	2.10	-	0.25	-	-1.22	-
	B	0.30	0.28	1.83	1.90	1.87	1.81	0.24	0.20	-1.24	-1.30
SAS-2A	Rip.	-	0.19		1.82		1.91		0.27		-1.45
SAS-1A	S	0.22	0.28	1.81	1.91	1.94	1.80	0.24	0.23	-1.34	-1.31
	B	0.26	0.31	1.84	2.01	1.90	1.35	0.23	0.17	-1.31	-1.39
TAS-3	S	0.19	0.22	1.79	1.80	2.18	1.97	0.31	0.22	-1.35	-1.32
TAS-13	S	0.22	0.29	1.83	2.07	1.97	1.20	0.24	0.16	-1.39	-1.50
TAS	Rip.	0.20	-	1.83	-	1.74	-	0.24	-	-1.37	-

Table 2 Calculated ratios and metrics to characterize the VOCs produced from the different experiments (O:C = oxygen-to-carbon ratio; H:C = hydrogen-to-carbon ratio, RDBE = ring double bond equivalent; AI_{mod} = modified aromaticity index; OS_c = carbon oxidation state).

Figure 5 shows the twenty most emitted photoproducts from all DOC and TOC samples. C_3H_6O (acetone or propanal) and $C_3H_8O_2$ (propylene glycol) were the two most abundant products detected in almost all samples, by concentration. In addition, C_2H_3N (acetonitrile), C_5H_8 (isoprene or cyclopentene), $C_5H_{12}O_2$ (1-propanol-3-ethoxy or diethoxymethane), C_8H_{10} (ethylbenzene or xylene) and $C_7H_8O_2$ (2-methoxyphenol or 4-methylcatechol) were often detected but in relatively low abundance.

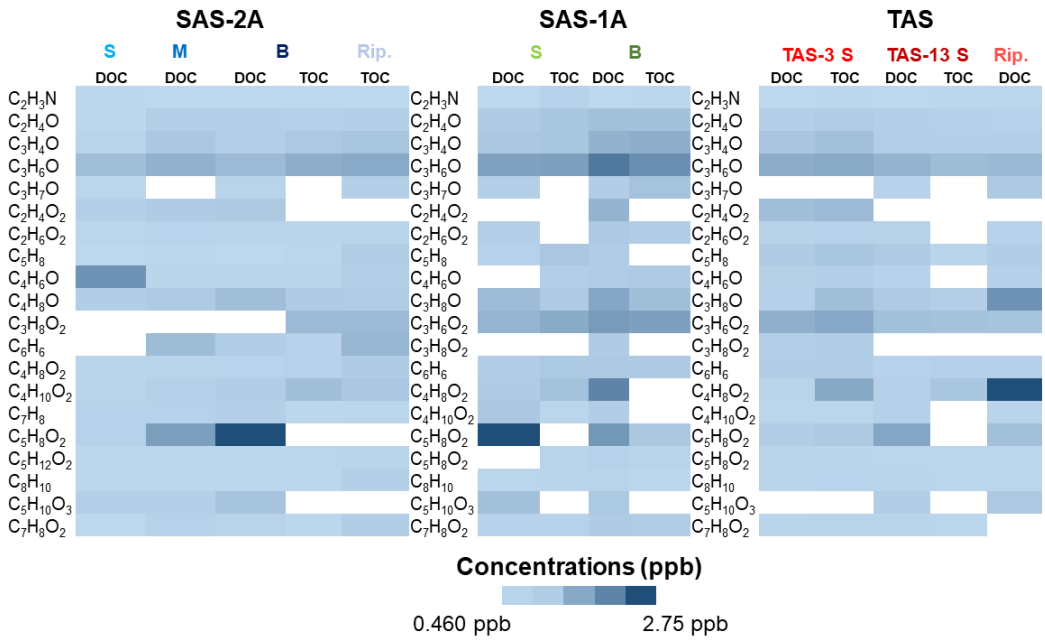

358

359 **Figure 5** Concentrations of the twenty most abundant VOCs produced in irradiation
360 experiments. White indicating no production (S = surface, M = middle, B = bottom, Rip. =
361 riparian).

362 All quantitative results are summarized in Table 3. C fluxes ranged between 1.93 and 9.47
363 μmol C m^{-2} d^{-1} for SAS and 1.58 and 8.71 μmol C m^{-2} d^{-1} for TAS. Both the number of
364 VOCs and the fluxes emitted were higher for samples collected from bottom waters. The
365 highest fluxes obtained were from SAS-2A (Bottom, DOC sample), which produced 9.47
366 μmol C m^{-2} d^{-1}. In general, irradiation of DOC samples led to more VOCs emitted as well
367 as greater concentrations and fluxes than TOC samples. Finally, in the oxic experiment,
368 there were 17 fewer species produced (29 compared to 46) than for its anoxic counterpart.
369 Furthermore, oxic conditions reduced the C fluxes almost 3-fold (1.93 compared to 5.06
370 μmol C m^{-2} d^{-1} under anoxic conditions).

371

372 Fluxes using the second approach (equation 4) are 1 to 2 orders of magnitude higher than
373 with the first approach.

374

Site/pond	ID	# of VOCs		Concentrations (ppb)		Fluxes (µmol C m^{-2} d^{-1})	
-	-	DOC	TOC	DOC	TOC	DOC	TOC
	S (anoxic)	46	-	0.655	-	5.06 (41.3)	-
	S (oxic)	29	-	0.460	-	1.93 (29.0)	-
SAS-2A	M	50	-	1.39	-	6.78 (87.5)	-
	B	59	35	2.76	1.28	9.47 (174)	4.27 (80.6)
SAS-2A	Rip.	53	-	2.42	-	9.45 (152)	-
SAS-1A	S	40	28	1.01	0.532	4.82 (63.6)	2.11 (33,5)
	B	53	24	1.44	0.856	6.20 (90.7)	2.59 (53.9)
TAS-3	S	54	60	1.79	2.29	6.70 (113)	8.71 (144)
TAS-13	S	49	20	0.932	0.388	4.65 (58.7)	1.58 (24.4)
TAS	Rip.	35	-	1.68	-	6.03 (106)	-

375 **Table 3** Summary of the quantitative results: number of VOCs, concentrations (ppb) and
376 fluxes (µmol C m^{-2} d^{-1}) from laboratory irradiations of water samples. Flux calculations
377 using Approach 2 (Equation 4, see text) are in parenthesis.

378

4. Discussion

4.1. Photoproduction of VOCs

Figure 3a–c suggests that the relatively high signal measured in the first 30-minute stabilization period prior to irradiation was diffusion of species naturally present at the time of sampling. However, this phenomenon is also observed for bottom and riparian samples, which are the least affected by light. It is also possible this is a residual signal from previous experiments in which semi-volatile compounds may have condensed onto the tubing and take time to flush. Irradiation of MilliQ water shows a similar pattern with relatively high signals in the first few minutes (Figure S4), giving support to the latter explanation. The same mechanism can also explain why the signal did not instantly drop when the lamp was shut off.

Following the onset of irradiation, the signal rose and reached a maximum, after which most signals started to decline, most likely as reactants were exhausted. However, some samples exhibited a constant increase in signal throughout the experiment. This may be due to the different volatilities of VOCs, or a reaction chain, whereby high molecular weight reactants produce lower molecular weight and more volatile reactants, whose photolysis in turn produces VOCs. Samples with greater aromaticity (high $SUVA_{254}$ values, Table 1) are expected to behave this way. To test this hypothesis, the aromatic-rich surface sample TAS-3 ($SUVA_{254}$ = 7.95 L mg C^{-1} m^{-1}) was irradiated overnight, and a maximum was eventually reached in the first 3 hours (Figure 3d). Although the experiment was not blank-subtracted, it was assumed that this would only affect the intensity of the signal, and not its general behavior (Figure S6). SAS-2A (riparian) is the other example of

a sample rich in aromatics that exhibited a constant photoreactivity during irradiation. Thus, the behavior appeared to be consistent across all samples, with the difference being the time required to photobleach all DOM.

4.2. Factors that control VOCs photoproduction

Our results point to four factors controlling VOC photoproduction: DOC quality, prior exposure to sunlight, presence of oxygen and presence of particulate matter.

A first factor that controls VOC photoproduction is the quality of the DOC. We observe that high concentrations of DOC did not lead to a greater diversity of VOCs. On the contrary, some of the dark-colored, DOC-rich ponds from SAS yielded fewer VOCs than the TAS ponds. Wang et al. [37] reached similar results and proposed that optical properties of the water could provide explanatory insights, an assertion we develop in this work. The three proxies used, namely a_{320}, $SUVA_{254}$ and Sr, give insight into the concentrations, aromatics and molecular size of CDOM, respectively. The surface water of every pond exhibited higher a_{320} values than bottom water, suggesting that CDOM strongly attenuates light and degrades into smaller moieties. Indeed, we observed that the irradiation of the DOC sample from TAS-3 (surface) produced the second-highest number of species (54 VOCs, Figure 4) and some of the highest fluxes detected (Table 3). Likewise, despite being the least concentrated in DOC and TOC, TAS-13's quantitative results were also among the highest. Since TAS-13 contains high amount of CDOM (a_{320} of 63.3 m^{-1}) characterized by large (Sr of 0.54, Table 1) and aromatics ($SUVA_{254}$ of 7.60 L mg C^{-1} m^{-1}, Table 1) molecules, these three proxies collectively point towards high photoreactivity. This suggests that the aromaticity ($SUVA_{254}$) and chromophoric properties of DOM (a_{320} and Sr) were better predictors of the number of VOCs that can be photoproduced than

concentration of DOC alone. This is in line with a recent study that reported a strong relationship between $SUVA_{254}$ and electron-donating capacity, a property useful to predict DOM photoreactivity [62]. Other authors found similar correlations that pointed to the importance of aromatics [63, 64] and molecular weight [63] as enablers of photochemistry.

A second factor that appeared to govern photoproduction of VOCs in our experiments was the extent to which the water sample was previously exposed to sunlight. We draw this conclusion from the observation that the irradiation of riparian waters led to some of the highest fluxes calculated in this work with values of 9.45 and 6.03 μmol C m^{-2} d^{-1} for the riparian zones of SAS-2A and TAS ponds, respectively (Table 3). Likewise, samples retrieved at the surface were always less productive in terms of the number of VOCs than samples retrieved from the bottom water, which we ascribe to exposure to sunlight prior to sampling.

A third factor was the presence of dissolved oxygen in the samples. We observed lower fluxes and a lower number of VOCs produced under oxygenated conditions compared to anoxic conditions (Table 3). Consequently, the fluxes measured under anoxic conditions could be upper limits of natural values, since those thermokarst systems may be thoroughly mixed during turnover events in the spring and fall, thus aerating the water column. The effects of dissolved oxygen on photochemistry are well documented, as O_2 allows chemical pathways that involve reactive oxygen species (ROS, e.g., H_2O_2, OH) [10]. Specifically, Cory et al. (2010) highlighted how reactive singlet oxygen ($^1O_2$) is key in the partial photo-oxidation of DOM which forms compounds with incorporated O atoms and which have a lower volatility.

Lastly, a fourth factor concerns sample filtration since POC can participate to photochemistry [65]. Our results showed that, excluding TAS-3 (surface), all DOC samples produced a higher number of species (Figure 4) along with greater fluxes (Table 3) than the POC samples. A combination of factors could explain these results. First, light scattering by particles could minimize light penetration and thus, photodegradation. Complex particle–organic interactions likely enable adsorption of VOCs onto particles, hence impeding their emission to the gas phase [66]. Furthermore, other photo-induced processes, such as POC photo-dissolution into DOC, are possible [65]. These concurrent reactions could reduce the number of reactants available for photolysis and explain the observed lower species counts and fluxes. Finally, we cannot rule out that our TOC samples became partially degraded during their 4-month storage at 4 °C. Since this was not tested by optical characterization, it cannot be quantified. A more precise evaluation of the role of POC is needed in future research.

4.3. Significance for the Arctic Environment

Up to now, most studies have focused on emissions of CO_2 and CH_4 from thermokarst ponds and highlighted their quantitative role in GHG emissions from thawing permafrost landscapes. At our study sites, Matveev et al. [33] calculated fluxes of CO_2 and CH_4 from SAS-1A and SAS-2A during the summer. In SAS-1A, their results show values of 1–12.8 mmol C m^{-2} d^{-1} for CH_4 and 4–55 mmol C m^{-2} d^{-1} for CO_2. For SAS-2A, it ranged between 1–10 mmol C m^{-2} d^{-1} for CH_4 and 20–242 mmol C m^{-2} d^{-1} for CO_2. These values are in the same range as those obtained in a study of 106 ponds in a wetland thermokarst system on Bylot Island (73°N, Nunavut) [32]. On Bylot Island, CH_4 fluxes varied between 0.03–5.82 mmol C m^{-2} d^{-1} and CO_2 fluxes between –11.78 (thus representing an uptake from the

469 atmosphere) and 65.5 mmol C m^{-2} d^{-1}. By comparison, even though the laboratory
470 experiments conducted here did not perfectly reproduce field conditions, the fluxes of C
471 from VOCs were generally 3 to 4 orders of magnitude lower than those documented above.
472 This indicates that VOCs are a small source of carbon in the arctic environment, with fluxes
473 of CO_2 > CH_4 >> VOCs.

474 In this study, we compare two approaches to upscale VOCs fluxes from the experimental
475 device to those prevailing above the ponds. Results show that considering CDOM
476 absorption - and not only the total light available - in addition to the water column
477 attenuation, yield higher fluxes than those obtained by solely extrapolating the absorption
478 at the air-water interface (Table 3). While the former approximation yields values closer to
479 the CO_2 and CH_4 emissions presented earlier, they remain 2-3 orders of magnitude lower.
480 As the apparent quantum yield could not be calculated for individual VOC due to the PTR-
481 MS limitations in molecular assignment, we believe the latter approach provides a more
482 precise assessment of VOCs photoproduction that should be employed for future research.

483 Other studies measured VOCs released directly from soils in permafrost organic-rich
484 peatlands and found emission rates ranging between 88.5 and 260.9 μg m^{-2} h^{-1} [21]. Using an
485 average VOC molecular mass of 70 g mol^{-1} in our experiments and correcting for the
486 proportion of carbon in each molecular composition, we calculated values of 7.09 and 42.5
487 μg m^{-2} h^{-1} for the lowest (TAS-13, surface, TOC) and the highest (SAS-2A, bottom, DOC)
488 emitting samples, respectively. Those results were 1–2 orders of magnitude lower than the
489 emission fluxes reported by Jiao et al. [21] These comparisons show how the Arctic
490 landscapes contain important VOCs sources. The results presented here suggest that the
491 contribution from microbial decomposition of soil organic matter in permafrost is more

important than that from CDOM photodegradation in thermokarst ponds. In addition, our results do not include the contribution of visible light in VOCs photoproduction. While CDOM absorption of visible light is less important than that of UV light in the water column (Bowen et al., 2020), it could still account for a non-negligible fraction of VOC fluxes. This knowledge gap should be addressed in future research.

4.4. Implication for Atmospheric Chemistry and Climate

While our results show that VOC production from thermokarst pond photochemistry makes a small contribution to C emissions to the atmosphere, they also point to a release of an array of reactive organic molecules in the atmosphere. The overlooked source of VOCs presented in this work might contribute to the local formation of atmospheric particles. The complex role of VOCs as SOA precursors depends on the volatility and solubility of the oxidation products [26]. For instance, the atmospheric oxidation of aromatic compounds such as cycloalkanes and cycloalkenes produces molecules containing polar functional groups, making them an important class of SOA precursor [26]. Based on Table 2, VOCs from SAS-2A experiments were unsaturated (RDBE between 1.81–2.10, AI_{mod} between 0.20–0.25) and the fluxes from aromatics (e.g., benzene, toluene, xylene) are relatively high (Figure 5, Figure S7). The greater fluxes of aromatics and oxygenated VOCs (Figure S7) contrast with previous similar work using the Vocus [18, 21]. This suggests that VOCs from thermokarst pond photochemistry could have a greater effect on SOA than other sources of VOC emissions. Although we did not have the data to quantitatively estimate the albedo change [67] and the associated radiative forcing, aerosol formation from the VOC emissions reported here could be high enough to affect the climate.

514 Laboratory and field studies on isoprene (2-methyl-1,3-butadiene, C_5H_8) demonstrated its
515 significant potential to produce both SOAs and O_3 in the presence of acidic particles due
516 to rapid reactivity with hydroxyl radicals (reaction lifetime of 1.7 hours) [68]. Some authors
517 have emphasized the importance of monitoring new sources of isoprene in the atmosphere,
518 especially in unpolluted environments [69, 70]. In this work, a product ion with the formula
519 $C_5H_9^+$, tentatively assigned to the protonated form of isoprene, was consistently prevalent
520 among emitted VOCs, especially in TAS samples (Figure 5 and Figure S7). These results
521 showed that thermokarst ponds photochemistry produced key reactive organic molecules
522 that may affect ozone production and radical concentrations.

523 **5. Conclusions**

524 Continuing permafrost thaw will increase export of terrestrial organic materials, rich in
525 aromatics and with limited sunlight exposure, to northern inland waters [71]. While the exact
526 magnitude of DOC photo-processing is debated [8, 72, 73], some studies have documented an
527 increased photolability of DOC draining from permafrost [11, 74]. Considering the anticipated
528 increase in the surface area of water bodies within the permafrost landscape [75], we argue
529 that closer monitoring of the emission levels and diversity of VOCs from thermokarst
530 ponds is needed.

531 We provide evidence for the photo emission of between 35 and 59 compounds to the gas
532 phase when DOM samples were exposed to actinic irradiation. The quality of the DOM
533 emerged as a key quantitative factor to control VOC photoproduction. VOC fluxes ranged
534 between 1.93 and 9.47 μmol C m^{-2} d^{-1}. This is 3 to 4 orders of magnitude lower than the
535 fluxes of CO_2 and CH_4 in similar thermokarst systems. It was also 1 to 2 orders of

magnitude lower than the VOCs fluxes from organic-rich soils in permafrost environments. In accordance with our earlier research[37], we conclude that although VOCs represent a small contribution to C emissions from surface water to the atmosphere in the Arctic, sunlight-induced VOCs might disproportionally impact atmospheric chemistry and, possibly, the climate.

6. Supporting information

Details on gas phase analysis, calibration curve, modeled spectral irradiance at the site, supplemental results on irradiance experiments, fluxes of VOC classes and candidate molecules detected by PTR-ToF-MS.

7. Acknowledgements

We acknowledge P. Audet for assistance with analytical work and G. St-Pierre for help on the field. We also thank the Centre for northern studies (CEN) that provided us with the research facilities in Umiujaq and Whapmagoostui-Kuujjuarapik and I. Laurion for insights on the TAS sampling sites. RMC acknowledges funding from the Sentinel North and Global Water Future programs funded in part by the Canada First Apogee Research Funds, and from the Advancing Climate Change Science in Canada program. DF acknowledges Natural Sciences and Engineering Research Council of Canada (NSERC), the Northern Scientific Training Program (NSTP) and the Fonds de recherche du Québec – Nature et technologies (FRQNT) for scholarships.

8. References

(1) Rantanen, M.; Karpechko, A. Y.; Lipponen, A.; Nordling, K.; Hyvärinen, O.; Ruosteenoja, K.; Vihma, T.; Laaksonen, A. The Arctic has warmed nearly four times faster than the globe since 1979. *Communications Earth & Environment* **2022**, *3* (1), 168.

(2) Rowland, J.; Jones, C.; Altmann, G.; Bryan, R.; Crosby, B.; Hinzman, L.; Kane, D.; Lawrence, D.; Mancino, A.; Marsh, P. Arctic landscapes in transition: responses to thawing permafrost. *Eos, Transactions American Geophysical Union* **2010**, *91* (26), 229-230.

(3) Vonk, J. E.; Tank, S. E.; Bowden, W. B.; Laurion, I.; Vincent, W. F.; Alekseychik, P.; Amyot, M.; Billet, M.; Canário, J.; Cory, R. M. Reviews and syntheses: Effects of permafrost thaw on Arctic aquatic ecosystems. *Biogeosciences* **2015**, *12* (23), 7129-7167.

(4) Hugelius, G.; Strauss, J.; Zubrzycki, S.; Harden, J. W.; Schuur, E.; Ping, C.-L.; Schirrmeister, L.; Grosse, G.; Michaelson, G. J.; Koven, C. D. Estimated stocks of circumpolar permafrost carbon with quantified uncertainty ranges and identified data gaps. *Biogeosciences* **2014**, *11* (23), 6573-6593.

(5) Schuur, E. A.; McGuire, A. D.; Schädel, C.; Grosse, G.; Harden, J.; Hayes, D. J.; Hugelius, G.; Koven, C. D.; Kuhry, P.; Lawrence, D. M. Climate change and the permafrost carbon feedback. *Nature* **2015**, *520* (7546), 171-179.

(6) Cory, R. M.; Ward, C. P.; Crump, B. C.; Kling, G. W. Sunlight controls water column processing of carbon in arctic fresh waters. *Science* **2014**, *345* (6199), 925-928.

(7) Koehler, B.; Landelius, T.; Weyhenmeyer, G. A.; Machida, N.; Tranvik, L. J. Sunlight-induced carbon dioxide emissions from inland waters. *Global Biogeochemical Cycles* **2014**, *28* (7), 696-711. DOI: 10.1002/2014GB004850.

(8) Laurion, I.; Massicotte, P.; Mazoyer, F.; Negandhi, K.; Mladenov, N. Weak mineralization despite strong processing of dissolved organic matter in Eastern Arctic tundra ponds. *Limnology and Oceanography* **2021**, *66*, S47-S63.

(9) Mazoyer, F.; Laurion, I.; Rautio, M. The dominant role of sunlight in degrading winter dissolved organic matter from a thermokarst lake in a subarctic peatland. *Biogeosciences* **2022**, *19* (17), 3959-3977.

(10) Cory, R. M.; McNeill, K.; Cotner, J. P.; Amado, A.; Purcell, J. M.; Marshall, A. G. Singlet oxygen in the coupled photochemical and biochemical oxidation of dissolved organic matter. *Environmental Science & Technology* **2010**, *44* (10), 3683-3689.

(11) Ward, C. P.; Cory, R. M. Complete and partial photo-oxidation of dissolved organic matter draining permafrost soils. *Environmental science & technology* **2016**, *50* (7), 3545-3553.

(12) Stubbins, A.; Spencer, R. G.; Chen, H.; Hatcher, P. G.; Mopper, K.; Hernes, P. J.; Mwamba, V. L.; Mangangu, A. M.; Wabakanghanzi, J. N.; Six, J. Illuminated darkness: Molecular signatures of Congo River dissolved organic matter and its photochemical alteration as revealed by ultrahigh precision mass spectrometry. *Limnology and Oceanography* **2010**, *55* (4), 1467-1477.

(13) Ward, C. P.; Cory, R. M. Assessing the prevalence, products, and pathways of dissolved organic matter partial photo-oxidation in arctic surface waters. *Environmental Science: Processes & Impacts* **2020**, *22* (5), 1214-1223.

(14) Cory, R. M.; Harrold, K. H.; Neilson, B. T.; Kling, G. W. Controls on dissolved organic matter (DOM) degradation in a headwater stream: the influence of photochemical and hydrological conditions in determining light-limitation or substrate-limitation of photo-degradation. *Biogeosciences* **2015**, *12* (22), 6669-6685. DOI: 10.5194/bg-12-6669-2015.

(15) Moran, M. A.; Zepp, R. G. Role of photoreactions in the formation of biologically labile compounds from dissolved organic matter. *Limnology and oceanography* **1997**, *42* (6), 1307-1316.

(16) Brüggemann, M.; Hayeck, N.; Bonnineau, C.; Pesce, S.; Alpert, P. A.; Perrier, S.; Zuth, C.; Hoffmann, T.; Chen, J.; George, C. Interfacial photochemistry of biogenic surfactants: a major source of abiotic volatile organic compounds. *Faraday Discussions* **2017**, *200* (0), 59-74, 10.1039/C7FD00022G. DOI: 10.1039/C7FD00022G.

(17) Atkinson, R.; Arey, J. Atmospheric degradation of volatile organic compounds. *Chemical reviews* **2003**, *103* (12), 4605-4638.

(18) Li, H.; Väliranta, M.; Mäki, M.; Kohl, L.; Sannel, A. B. K.; Pumpanen, J.; Koskinen, M.; Bäck, J.; Bianchi, F. Overlooked organic vapor emissions from thawing Arctic permafrost. *Environmental Research Letters* **2020**, *15* (10), 104097.
(19) Kramshøj, M.; Albers, C. N.; Holst, T.; Holzinger, R.; Elberling, B.; Rinnan, R. Biogenic volatile release from permafrost thaw is determined by the soil microbial sink. *Nature Communications* **2018**, *9* (1), 3412. DOI: 10.1038/s41467-018-05824-y.
(20) Kramshøj, M.; Albers, C. N.; Svendsen, S. H.; Björkman, M. P.; Lindwall, F.; Björk, R. G.; Rinnan, R. Volatile emissions from thawing permafrost soils are influenced by meltwater drainage conditions. *Global change biology* **2019**, *25* (5), 1704-1716.
(21) Jiao, Y.; Davie-Martin, C. L.; Kramshøj, M.; Christiansen, C. T.; Lee, H.; Althuizen, I. H.; Rinnan, R. Volatile organic compound release across a permafrost-affected peatland. *Geoderma* **2023**, *430*, 116355.
(22) Creamean, J. M.; Hill, T. C.; DeMott, P. J.; Uetake, J.; Kreidenweis, S.; Douglas, T. A. Thawing permafrost: an overlooked source of seeds for Arctic cloud formation. *Environmental Research Letters* **2020**, *15* (8), 084022.
(23) Abbatt, J. P.; Leaitch, W. R.; Aliabadi, A. A.; Bertram, A. K.; Blanchet, J.-P.; Boivin-Rioux, A.; Bozem, H.; Burkart, J.; Chang, R. Y.; Charette, J. Overview paper: New insights into aerosol and climate in the Arctic. *Atmospheric Chemistry and Physics* **2019**, *19* (4), 2527-2560.
(24) Mungall, E. L.; Abbatt, J. P.; Wentzell, J. J.; Lee, A. K.; Thomas, J. L.; Blais, M.; Gosselin, M.; Miller, L. A.; Papakyriakou, T.; Willis, M. D. Microlayer source of oxygenated volatile organic compounds in the summertime marine Arctic boundary layer. *Proceedings of the National Academy of Sciences* **2017**, *114* (24), 6203-6208.
(25) Maria, S. F.; Russell, L. M.; Gilles, M. K.; Myneni, S. C. Organic aerosol growth mechanisms and their climate-forcing implications. *Science* **2004**, *306* (5703), 1921-1924.
(26) Hallquist, M.; Wenger, J. C.; Baltensperger, U.; Rudich, Y.; Simpson, D.; Claeys, M.; Dommen, J.; Donahue, N.; George, C.; Goldstein, A. The formation, properties and impact of secondary organic aerosol: current and emerging issues. *Atmospheric chemistry and physics* **2009**, *9* (14), 5155-5236.
(27) Twomey, S. The influence of pollution on the shortwave albedo of clouds. *Journal of the atmospheric sciences* **1977**, *34* (7), 1149-1152.
(28) Carter, W. P. Development of ozone reactivity scales for volatile organic compounds. *Air & waste* **1994**, *44* (7), 881-899.
(29) Finlayson-Pitts, B.; Pitts Jr, J. Atmospheric chemistry of tropospheric ozone formation: scientific and regulatory implications. *Air & Waste* **1993**, *43* (8), 1091-1100.
(30) Serikova, S.; Pokrovsky, O.; Laudon, H.; Krickov, I.; Lim, A.; Manasypov, R.; Karlsson, J. High carbon emissions from thermokarst lakes of Western Siberia. *Nature Communications* **2019**, *10* (1), 1552.
(31) Cory, R. M.; Crump, B. C.; Dobkowski, J. A.; Kling, G. W. Surface exposure to sunlight stimulates CO2 release from permafrost soil carbon in the Arctic. *Proceedings of the National Academy of Sciences* **2013**, *110* (9), 3429-3434.
(32) Bouchard, F.; Laurion, I.; Prėskienis, V.; Fortier, D.; Xu, X.; Whiticar, M. J. Modern to millennium-old greenhouse gases emitted from ponds and lakes of the Eastern Canadian Arctic (Bylot Island, Nunavut). *Biogeosciences* **2015**, *12* (23), 7279-7298.
(33) Matveev, A.; Laurion, I.; Deshpande, B. N.; Bhiry, N.; Vincent, W. F. High methane emissions from thermokarst lakes in subarctic peatlands. *Limnology and Oceanography* **2016**, *61* (S1), S150-S164.
(34) Pozzer, A. C.; Gómez, P. A.; Weiss, J. Volatile organic compounds in aquatic ecosystems–Detection, origin, significance and applications. *Science of The Total Environment* **2022**, *838*, 156155.
(35) Spencer, R. G.; Stubbins, A.; Hernes, P. J.; Baker, A.; Mopper, K.; Aufdenkampe, A. K.; Dyda, R. Y.; Mwamba, V. L.; Mangangu, A. M.; Wabakanghanzi, J. N. Photochemical degradation of dissolved organic matter and dissolved lignin phenols from the Congo River. *Journal of Geophysical Research: Biogeosciences* **2009**, *114* (G3).
(36) Ward, C. P.; Sleighter, R. L.; Hatcher, P. G.; Cory, R. M. Insights into the complete and partial photooxidation of black carbon in surface waters. *Environmental Science: Processes & Impacts* **2014**, *16* (4), 721-731.

(37) Wang, T.; Kalalian, C.; Fillion, D.; Perrier, S.; Chen, J.; Domine, F.; Zhang, L.; George, C. Sunlight Induces the Production of Atmospheric Volatile Organic Compounds (VOCs) from Thermokarst Ponds. *Environmental Science & Technology* **2023**, *57* (45), 17363-17373. DOI: 10.1021/acs.est.3c03303.
(38) Gagnon, M.; Domine, F.; Boudreau, S. The carbon sink due to shrub growth on Arctic tundra: a case study in a carbon-poor soil in eastern Canada. *Environmental Research Communications* **2019**, *1* (9), 091001.
(39) Bhiry, N.; Delwaide, A.; Allard, M.; Bégin, Y.; Filion, L.; Lavoie, M.; Nozais, C.; Payette, S.; Pienitz, R.; Saulnier-Talbot, É. Environmental change in the Great Whale River region, Hudson Bay: Five decades of multidisciplinary research by Centre d'études nordiques (CEN). *Ecoscience* **2011**, *18* (3), 182-203.
(40) Natural Ressources Canada. *The Atlas of Canada - Open Maps*. https://search.open.canada.ca/openmap/957782bf-847c-4644-a757-e383c0057995 (accessed 20 Feb. 2024).
(41) Wauthy, M.; Rautio, M.; Christoffersen, K. S.; Forsström, L.; Laurion, I.; Mariash, H. L.; Peura, S.; Vincent, W. F. Increasing dominance of terrigenous organic matter in circumpolar freshwaters due to permafrost thaw. *Limnology and Oceanography Letters* **2018**, *3* (3), 186-198.
(42) Folhas, D.; Duarte, A. C.; Pilote, M.; Vincent, W. F.; Freitas, P.; Vieira, G.; Silva, A. M. S.; Duarte, R. M. B. O.; Canário, J. Structural Characterization of Dissolved Organic Matter in Permafrost Peatland Lakes. *Water* **2020**, *12* (11), 3059. DOI: 10.3390/w12113059.
(43) Laurion, I.; Mladenov, N. Dissolved organic matter photolysis in Canadian arctic thaw ponds. *Environmental Research Letters* **2013**, *8* (3), 035026. DOI: 10.1088/1748-9326/8/3/035026.
(44) Weishaar, J. L.; Aiken, G. R.; Bergamaschi, B. A.; Fram, M. S.; Fujii, R.; Mopper, K. Evaluation of Specific Ultraviolet Absorbance as an Indicator of the Chemical Composition and Reactivity of Dissolved Organic Carbon. *Environmental Science & Technology* **2003**, *37* (20), 4702-4708. DOI: 10.1021/es030360x.
(45) Helms, J. R.; Stubbins, A.; Ritchie, J. D.; Minor, E. C.; Kieber, D. J.; Mopper, K. Absorption spectral slopes and slope ratios as indicators of molecular weight, source, and photobleaching of chromophoric dissolved organic matter. *Limnology and oceanography* **2008**, *53* (3), 955-969.
(46) Massicotte, P.; Markager, S. Using a Gaussian decomposition approach to model absorption spectra of chromophoric dissolved organic matter. *Marine chemistry* **2016**, *180*, 24-32.
(47) Roveretto, M.; Li, M.; Hayeck, N.; Brüggemann, M.; Emmelin, C.; Perrier, S.; George, C. Real-Time Detection of Gas-Phase Organohalogens from Aqueous Photochemistry Using Orbitrap Mass Spectrometry. *ACS Earth and Space Chemistry* **2019**, *3* (3), 329-334. DOI: 10.1021/acsearthspacechem.8b00209.
(48) Yager, J. E.; Yue, C. D. Evaluation of the xenon arc lamp as a light source for aquatic photodegradation studies: Comparison with natural sunlight. *Environmental Toxicology and Chemistry: An International Journal* **1988**, *7* (12), 1003-1011.
(49) Deshpande, B. N.; MacIntyre, S.; Matveev, A.; Vincent, W. F. Oxygen dynamics in permafrost thaw lakes: Anaerobic bioreactors in the C anadian subarctic. *Limnology and Oceanography* **2015**, *60* (5), 1656-1670.
(50) Bouchard, F.; Francus, P.; Pienitz, R.; Laurion, I.; Feyte, S. Subarctic thermokarst ponds: Investigating recent landscape evolution and sediment dynamics in thawed permafrost of northern Québec (Canada). *Arctic, Antarctic, and Alpine Research* **2014**, *46* (1), 251-271.
(51) Prairie, Y.; Breton, J.; Vallières, C.; Laurion, I. Limnological properties of permafrost thaw ponds in northeastern Canada. *Canadian Journal of Fisheries and Aquatic Sciences* **2009**, *66* (10), 1635-1648. DOI: 10.1139/f09-108.
(52) Li, H.; Riva, M.; Rantala, P.; Heikkinen, L.; Daellenbach, K.; Krechmer, J. E.; Flaud, P.-M.; Worsnop, D.; Kulmala, M.; Villenave, E. Terpenes and their oxidation products in the French Landes forest: insights from Vocus PTR-TOF measurements. *Atmospheric Chemistry and Physics* **2020**, *20* (4), 1941-1959.
(53) Krechmer, J.; Lopez-Hilfiker, F.; Herndon, S. C.; Koss, A.; Canagaratna, M. R.; Majluf, F.; Hutterli, M.; Stoermer, C.; Deming, B.; Kimmel, J. Performance Evaluation and Field Deployment of a Novel Vocus PTR-TOF for Quantification, Identification, and Apportionment of Gaseous Air Pollutants. In *AGU Fall Meeting Abstracts*, 2018; Vol. 2018, pp A33G-3201.
(54) Stark, H.; Yatavelli, R. L.; Thompson, S. L.; Kimmel, J. R.; Cubison, M. J.; Chhabra, P. S.; Canagaratna, M. R.; Jayne, J. T.; Worsnop, D. R.; Jimenez, J. L. Methods to extract molecular and bulk chemical information

from series of complex mass spectra with limited mass resolution. *International Journal of Mass Spectrometry* **2015**, *389*, 26-38.
(55) Cubison, M.; Jimenez, J. Statistical precision of the intensities retrieved from constrained fitting of overlapping peaks in high-resolution mass spectra. *Atmospheric Measurement Techniques* **2015**, *8* (6), 2333-2345.
(56) Coggon, M. M.; Stockwell, C. E.; Claflin, M. S.; Pfannerstill, E. Y.; Lu, X.; Gilman, J. B.; Marcantonio, J.; Cao, C.; Bates, K.; Gkatzelis, G. I. Identifying and correcting interferences to PTR-ToF-MS measurements of isoprene and other urban volatile organic compounds. *EGUsphere* **2023**, *2023*, 1-41.
(57) Cappellin, L.; Karl, T.; Probst, M.; Ismailova, O.; Winkler, P. M.; Soukoulis, C.; Aprea, E.; Märk, T. D.; Gasperi, F.; Biasioli, F. On quantitative determination of volatile organic compound concentrations using proton transfer reaction time-of-flight mass spectrometry. *Environmental science & technology* **2012**, *46* (4), 2283-2290.
(58) Sekimoto, K.; Li, S.-M.; Yuan, B.; Koss, A.; Coggon, M.; Warneke, C.; de Gouw, J. Calculation of the sensitivity of proton-transfer-reaction mass spectrometry (PTR-MS) for organic trace gases using molecular properties. *International Journal of Mass Spectrometry* **2017**, *421*, 71-94.
(59) Yuan, B.; Koss, A. R.; Warneke, C.; Coggon, M.; Sekimoto, K.; de Gouw, J. A. Proton-transfer-reaction mass spectrometry: applications in atmospheric sciences. *Chemical reviews* **2017**, *117* (21), 13187-13229.
(60) Finlayson-Pitts, B. J.; Pitts Jr, J. N. Atmospheric chemistry. Fundamentals and experimental techniques. **1986**.
(61) Lackner, G.; Domine, F.; Sarrazin, D.; Nadeau, D.; Belke-Brea, M. Hydrometeorological, snow and soil data from a low-Arctic valley in the forest-tundra ecotone in Northern Quebec. PANGAEA. 2022.
(62) Berg, S. M.; Wammer, K. H.; Remucal, C. K. Dissolved Organic Matter Photoreactivity Is Determined by Its Optical Properties, Redox Activity, and Molecular Composition. *Environmental Science & Technology* **2023**.
(63) Maizel, A. C.; Li, J.; Remucal, C. K. Relationships Between Dissolved Organic Matter Composition and Photochemistry in Lakes of Diverse Trophic Status. *Environmental Science & Technology* **2017**, *51* (17), 9624-9632. DOI: 10.1021/acs.est.7b01270.
(64) Berg, S. M.; Whiting, Q. T.; Herrli, J. A.; Winkels, R.; Wammer, K. H.; Remucal, C. K. The role of dissolved organic matter composition in determining photochemical reactivity at the molecular level. *Environmental Science & Technology* **2019**, *53* (20), 11725-11734.
(65) Hu, B.; Wang, P.; Wang, C.; Bao, T. Photogeochemistry of particulate organic matter in aquatic systems: A review. *Science of The Total Environment* **2022**, *806*, 150467. DOI: https://doi.org/10.1016/j.scitotenv.2021.150467.
(66) He, W.; Chen, M.; Schlautman, M. A.; Hur, J. Dynamic exchanges between DOM and POM pools in coastal and inland aquatic ecosystems: A review. *Science of the Total Environment* **2016**, *551*, 415-428.
(67) Charlson, R. J.; Lovelock, J. E.; Andreae, M. O.; Warren, S. G. Oceanic phytoplankton, atmospheric sulphur, cloud albedo and climate. *Nature* **1987**, *326* (6114), 655-661.
(68) Kroll, J. H.; Ng, N. L.; Murphy, S. M.; Flagan, R. C.; Seinfeld, J. H. Secondary organic aerosol formation from isoprene photooxidation. *Environmental science & technology* **2006**, *40* (6), 1869-1877.
(69) Seco, R.; Holst, T.; Matzen, M. S.; Westergaard-Nielsen, A.; Li, T.; Simin, T.; Jansen, J.; Crill, P.; Friborg, T.; Rinne, J. Volatile organic compound fluxes in a subarctic peatland and lake. *Atmospheric Chemistry and Physics* **2020**, *20* (21), 13399-13416.
(70) Steinke, M.; Hodapp, B.; Subhan, R.; Bell, T. G.; Martin-Creuzburg, D. Flux of the biogenic volatiles isoprene and dimethyl sulfide from an oligotrophic lake. *Scientific reports* **2018**, *8* (1), 1-10.
(71) Liebner, S.; Welte, C. U. Roles of thermokarst lakes in a warming world. *Trends in Microbiology* **2020**, *28* (9), 769-779.
(72) Stubbins, A.; Mann, P. J.; Powers, L.; Bittar, T. B.; Dittmar, T.; McIntyre, C. P.; Eglinton, T. I.; Zimov, N.; Spencer, R. G. Low photolability of yedoma permafrost dissolved organic carbon. *Journal of Geophysical Research: Biogeosciences* **2017**, *122* (1), 200-211.

(73) Shirokova, L. S.; Chupakov, A. V.; Zabelina, S. A.; Neverova, N. V.; Payandi-Rolland, D.; Causserand, C.; Karlsson, J.; Pokrovsky, O. S. Humic surface waters of frozen peat bogs (permafrost zone) are highly resistant to bio-and photodegradation. *Biogeosciences* **2019**, *16* (12), 2511-2526.
(74) Panneer Selvam, B.; Lapierre, J.-F.; Guillemette, F.; Voigt, C.; Lamprecht, R. E.; Biasi, C.; Christensen, T. R.; Martikainen, P. J.; Berggren, M. Degradation potentials of dissolved organic carbon (DOC) from thawed permafrost peat. *Scientific Reports* **2017**, *7* (1), 45811.
(75) Paltan, H.; Dash, J.; Edwards, M. A refined mapping of Arctic lakes using Landsat imagery. *International Journal of Remote Sensing* **2015**, *36* (23), 5970-5982.

766 **For TOC Only**

767